Constraints on the Progenitor of Cassiopeia A

Patrick A. Young[1,2], Chris L. Fryer[1,3], Aimee Hungerford[1], David Arnett[2], Gabriel Rockefeller[1,3], F. X. Timmes[1], Benedict Voit[1,4], Casey Meakin[2], and Kristoffer A. Eriksen[1,2]

payoung@lanl.gov, fryer@lanl.gov, aimee@lanl.gov, darnett@as.arizona.edu, gaber@lanl.gov, fxt@lanl.gov, cmeakin@as.arizona.edu, keriksen@as.arizona.edu

ABSTRACT

We compare a suite of 3D explosion calculations and stellar models incorporating advanced physics with observational constraints on the progenitor of Cassiopeia A. We consider binary and single stars from 16 to 40 $M_{\odot}$ with a range of explosion energies and geometries. The parameter space allowed by observations of nitrogen rich high velocity ejecta, ejecta mass, compact remnant mass, and ^{44}Ti and ^{56}Ni abundances individually and as an ensemble is considered. A progenitor of 15-25 $M_{\odot}$ which loses its hydrogen envelope to a binary interaction and undergoes an energetic explosion can match all the observational constraints.

Subject headings: hydrodynamics—nucleosynthesis—stars: evolution—supernova remnants—supernovae: individual (Cassiopeia A)

1. INTRODUCTION

Cassiopeia A is perhaps the best studied young Galactic supernova Remnant (SNR). It is nearby (3.4 kpc) (Reed et al. 1995) and young ($\sim$ 325 yr) (Thorstensen, Fesen, & van den Bergh 2001). The wealth of data from ground-based observations in the optical, IR, and radio and from space in the optical, x-ray, and γ-ray allow us to study its morphology and composition in great detail, and even observe its secular evolution. This remnant offers

[1]Theoretical Astrophysics, Los Alamos National Laboratories, Los Alamos, NM 87545

[2]Steward Observatory, University of Arizona, Tucson AZ 85721

[3]Physics Dept., University of Arizona, Tucson AZ 85721

[4]Department of Computer Science, The University of Texas at Dallas, Richardson TX 75080

a unique opportunity to place constraints on both the explosion and the nature of the progenitor star. In this paper we will concentrate upon the latter.

The identity of Cas A's progenitor has been the subject of tremendous debate. Suggestions have ranged from a 16 $M_\odot$ single star (Chevalier & Oishi 2003) to various binary scenarios, to a Wolf-Rayet remnant of a very massive ($\leq$ 60 $M_\odot$) precursor (Fesen & Becker 1991). We must constrain the initial conditions far better if we are to use the large amount of information obtained from the remnant to understand the supernova explosion mechanism. It has also been suggested that Cas A is related to Oxygen-rich SNRs in the Magellanic Clouds or to Type Ib supernovae (Blair et al. 2000, i.e.). Again we must be certain of the progenitor's identity before accepting that Cas A is representative of a large class of supernovae.

Most estimates for a progenitor mass are derived from one or few lines of evidence. The lowest mass estimate of 16 $M_\odot$ by Chevalier & Oishi (2003) is arrived at through self-similarity solutions for the explosion, constrained by the positions of the forward and reverse shock and an assumption of the structure of the circumstellar medium. The highest masses estimates (Fesen & Becker 1991, i.e.) rest upon the lack of hydrogen in the ejecta and the Wolf-Rayet-like properties of the pre-SN mass loss deduced from the quasi-stationary flocculi. Though the highest mass estimates in the literature have dwindled towards the low end of the WR progenitor mass range (25-30 $M_\odot$), there is a lingering conception of Cas A as a "very massive star" in the community. Other attempts have been made to estimate a mass from nucleosynthetic products in the remnant. These estimates vary wildly due to the enormous variation in theoretical estimates of yields.

Most of these estimates contradict other lines of evidence than those upon which they are based. For example, Willingale et al. (2002) find that the ejecta abundance ratios match the yield from a star that is 12 $M_\odot$ at the time of the explosion. From spectral line fits to the same data, Willingale et al. (2003) estimate a total ejecta mass of 2.2 $M_\odot$. If, as seems likely, the compact remnant is a neutron star, the star must have been $\sim$ 4 $M_\odot$ at the time of explosion. Willingale et al. take care not to make two contradictory claims about the progenitor, but the case serves to illustrate the traps which may snare the unwary.

We attempt a different approach. We examine each of the major observational constraints in turn, and compare them with progenitor models. We then describe the parameter space allowed for the progenitor if each of the constraints is accepted. Each constraint allows a wide range of possibilities, but when the constraints are taken together, almost all of those possibilities are eliminated. Section 2 describes the progenitor models and explosion calculations. Section 3 evaluates the major observational constraints and their potential level of uncertainty. Section 4 evaluates our individual progenitor plus explosion calculations in

terms of the constraints. Section 5 describes the kinds of progenitors allowed by adopting the constraints and examines the implications for our understanding of Cas A and supernovae in general.

2. PROGENITOR AND EXPLOSION CALCULATIONS

2.1. Progenitors

We have produced four progenitor models as initial conditions for 3D explosion calculations: two single stars, $40M_{\odot}$ and $23M_{\odot}$, and two stars where the hydrogen envelope was removed during a red giant phase to mimic a common envelop evolution, $23M_{\odot}$ and $16M_{\odot}$. Although this sampling is sparse, it illustrates the effect of the observational constraints on the models and allow us to home in on the actual progenitor of Cas A.

All four models were produced with the TYCHO stellar evolution code (Young & Arnett 2005). In the absence of information on the composition of Cas A's progenitor, we use the Grevesse & Sauval (1998) solar abundances to ease later comparison with earlier calculations. The models are non-rotating and include hydrodynamic mixing processes (Young & Arnett 2005; Young et al. 2005). Rotation is a smaller effect than the hydrodynamic mixing in terms of core sizes, and therefore masses of material at various stages of nuclear processing, at core collapse. The magnitude of the effect of rotation becomes comparable to that of wave driven mixing only for massive stars rotating near breakup. The possibility remains that there is a strong interaction between rotation and internal waves, but the theoretical framework to evaluate this does not yet exist. In terms of internal structure, we consider rotation to be a perturbation on the existing hydrodynamic mixing smaller than the other uncertainties in the study. The main area in which rotation may have an important effect on this study is in enhancing the mass loss. Since mass loss in uncertain to begin with, we discuss below the possible impact of increased mass loss on our results. Angular momentum is also important to some supernova mechanisms, such as the jet driven model, but we do not use such a mechanism here. Explosion asymmetries which may be induced by rotation are examined in a parametrized way. Mass loss uses the prescriptions of Kudritzki et al. (1989) for OB mass loss, Blöcker (1995) for red giant/supergiant mass loss, and Lamers & Nugis (2003) for WR phases.

These progenitor models are an improvement over earlier studies, but much work remains to be done in stellar physics. While our description of the hydrodynamic mixing is unlikely to change qualitatively, it will change in detail as simulations improve our understanding. A good understanding of angular momentum transfer in stellar interiors is lacking.

Our picture of mass loss also has shortcomings, especially for cool stars. The effects of waves on the URCA process and neutrino cooling are not included, nor have wave-driven non-radial perturbations been imposed on the initial conditions for the explosion.

The 40 $M_\odot$ star develops an instability during the late main sequence which should lead to a Luminous Blue Variable (LBV) phase, so we remove 1 $M_\odot$ from the envelope as a conservative estimate for the mass lost in eruptions. This model develops a core of He plus triple α products with a maximum extent of 19 $M_\odot$ and a very thin (< 0.1 $M_\odot$ envelope of CNO burning products. Since N is rapidly destroyed at triple α temperatures, the N rich material disappears quickly as the thin CNO layer is removed by mass loss. The core is subsequently eroded by mass loss as a WC and then WO star. The final mass at collapse is 7.8 $M_\odot$.

The single 23 $M_\odot$ star evolves normally as a red supergiant. The final mass is 14.4 $M_\odot$, with a 5 $M_\odot$ H-rich envelope. The main uncertainty in this progenitor is the extent of red supergiant mass loss. Mass loss predictions for cool stars are based on empirical relations, not physical theories. Our rates are similar to those observed, but a factor of two change could be admissible. This star has a core of material with $\bar{\mathrm{A}} \geq 16$ of $\sim$6.5 $M_\odot$, with an additional 3 $M_\odot$ of material partially processed by triple α burning. The internal structure differs substantially from the 23 $M_\odot$ progenitor with a "binary event".

The 23 $M_\odot$ star with artificial binary evolution has its hydrogen envelope removed when the star is at the base of the first ascent red giant branch. At this point the radius exceeds 200 $R_\odot$, which is larger than the separation of many massive star binaries. The convective envelope has not reached the hydrogen burning shell, so the He core size and abundance profile of CNO products within the core are not modified. We do not attempt to change the structure of the star aside from removing the envelope. We can place some weak constraints on the nature of the companion assuming that the reason we do not see it is that it merged with the primary star during this common envelope phase. A companion of >0.9 $M_\odot$ could remove the entire hydrogen envelope assuming standard common envelope evolution and parameters (Fryer et al. 1998). At a separation of 200 $R_\odot$ a companion $\gtrsim 2.6$ $M_\odot$ will not merge. The maximum mass for a merger increases with decreasing separation.

If the companion is lower mass and still in hydrogen burning, the density contrast with the primary's core should be sufficiently large that the mixing of material between stars will be limited to Kelvin-Helmholtz instabilities at the interface with the accreted material if the companion merges. If we also assume the entropy barrier of the H burning shell limits the extent of any mixing process driven by a non-merger, our results will change little. We assume by necessity that the amount of mass accreted from the merger of a companion is small compared to the mass of the primary. Mass loss removes any residual H, and the star

evolves as a WNL and WN until core collapse. The final mass is 6.4 $M_\odot$, with a nitrogen-rich He envelope.

The 16 $M_\odot$ binary reaches a final mass of 5 $M_\odot$. At collapse there is a residual envelope of $\sim$ 0.01 $M_\odot$ with 30% hydrogen. A further 0.5 $M_\odot$ of material is completely H depleted but N enriched. A significant fraction of this material does not have CNO equilibrium abundances because of mixing of C/O rich material out from the He shell convective zone.

Figure 1 shows mean atomic weight $\bar{\mathrm{A}}$ (top) and density (bottom) vs. mass coordinate for the four progenitor models. The extreme mass loss of the 40 $M_\odot$ WR and the binaries results in lower densities in the oxygen dominated part of the core, compared to the 23 $M_\odot$ RSG. In the Fe-peak dominated core, the models with higher densities have lower Y_e. Most of the support in this region is supplied by electron pressure, so with fewer electrons per nucleon, the density must be higher to provide pressure support. Higher densities out to large mass coordinate in the 23 $M_\odot$ RSG will significantly delay the explosion, and will result in a weaker explosion for a given neutrino luminosity.

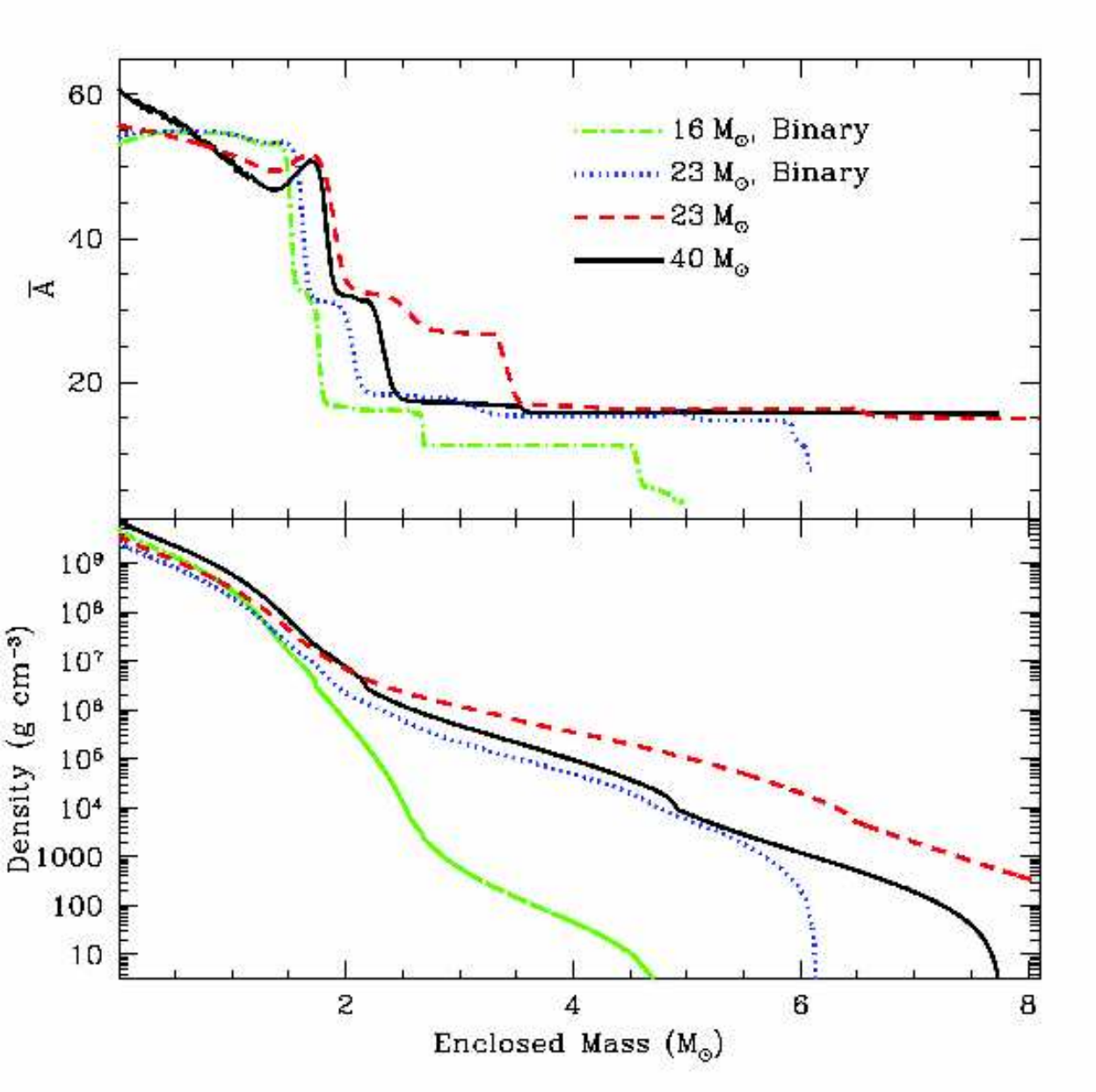

Fig. 1.— Mean atomic weight $\bar{A}$ (top) and density (bottom) vs. mass coordinate for the four progenitor models. The extreme mass loss of the 40 $M_\odot$ WR and the binaries result in lower densities in the oxygen dominated part of the core compared to the 23 $M_\odot$ RSG. In the Fe-peak dominated core the densities are higher because Y_e is lower.

2.2. Explosion Calculations

We model the explosion of these stars using a two-step process: the collapse and launch of the explosion modeled in 1-dimension and the propagation of the shock through the star modeled in 3-dimensions. The 1-dimensional code uses a coupled set of equations of state to model the wide range of densities in the collapse phase (see Herant et al. 1994; Fryer et al. 1999, for details) including a 14-element nuclear network (Benz, Thielemann, & Hills 1989) to follow the energy generation. This network terminates at ^{56}Ni and cannot follow neutron excess. A 512 element network was used in post-processing to derive more accurate yields. This code uses a flux-limited diffusion transport scheme for 3 species of neutrinos ($\nu_e, \bar{\nu}_e$, and $\nu_x = \mu$ and τ neutrinos) with a "trapping radius" defined as the position where optical depth out of the star for a given neutrino species is less than a given value. For the simulations presented here, this value is set to an optical depth of 0.1. We artificially raise the neutrino flux at this trapping radius to produce explosions of varying energies.

After the launch of the shock, we cut out the neutron star (replacing it with a hard reflective boundary and a gravitational potential defined by its baryonic mass). We continue to follow the explosion in 1-dimension until nuclear burning is finished (roughly 10-100 s after the launch of the explosion). At this point, the output from the 1-dimensional simulation is mapped into our 3D explosion code: SNSPH (Fryer et al. 2005). We follow the explosion with this code to study the mixing produced as the shock moves through the star. The amount of mixing both determines the final yield of the explosion and the spatial position of the elements relative to each other. It is this mixing that (hopefully) causes the inversion of some of the iron and silicon ejecta seen in the X-ray images (Hwang & Laming 2003).

As the focus of this paper is on the progenitor, we defer discussion of the actual spatial distribution and detailed nucleosynthesis of the ejecta to a later paper. Instead, we concentrate on the remnant and ejecta masses from our explosion calculations and bulk yields of ^{44}Ti and ^{56}Ni from minimal post-processing of the explosive nucleosynthesis. We have run 13 explosion calculations, using our 4 progenitors with different explosion energies and asymmetries. The asymmetric explosion is a sinusoidally varying jet explosion with a factor of 2 increase in the velocity along one axis (Hungerford, Fryer, & Warren 2003). The explosion energy is defined as the kinetic energy of the ejecta at the end of the simulation. Table 1 shows the results from this suite of simulations. There are a few important trends in these results.

First, note that the single-star progenitors (the 40 $M_\odot$ star and the single 23 $M_\odot$ star) require much higher explosion energies to avoid the formation of a black hole. The compact cores of these single stars are more difficult to explode. It is likely that, if they explode, they explode later with weaker explosions (Fryer 1999). Such weak explosions will always lead to

a lot of material falling back onto the compact remnant, forming a black hole. To avoid this fate, we must drive considerable energy into the gain region of the star. The explosion then occurs roughly at the same time as the lower mass progenitors, but because the explosion must overcome a higher ram pressure, it is much stronger. If we could show that the compact remnant from Cas A were a neutron star, then this would constrain both the progenitor and its explosion energy.

The more energetic explosions have stronger shocks which extend the explosion burning further out in the star. This increases the yield of many of the explosive burning products such as ^{56}Ni and ^{44}Ti. Upper limits on the ^{56}Ni and a measurement of the ^{44}Ti will also constrain our explosion energy and progenitor (§ 3.4).

Asymmetric explosions allow some wiggle room in these yield and compact remnant constraints. An asymmetric explosion of the same energy as a symmetric explosion will eject more heavy elements, but produce a larger compact remnant. Where the explosion is weaker than the symmetric explosion, the material is more likely to fall back and increase the mass of the compact remnant. Where the explosion is stronger, there is increased burning and mixing. Table 1 shows the increased yield just from the increased mixing. Asymmetries can dramatically change the heavy element yield.

3. OBSERVATIONAL CONSTRAINTS ON PROGENITOR MODELS

There are a variety of constraints on the possible progenitor arising from observations of Cas A itself. Some of these are considerably more stringent than others. In this section we examine the nature and strength of the major constraints. We then apply these constraints on our specific simulations in §4, and then to general stars in §5.

3.1. Nitrogen Knots

There are some four dozen observed high velocity nitrogen-rich knots in Cas A (Fesen 2001). As the supernova shock moves through the star, the nitrogen layer is accelerated. Because nitrogen is an efficient coolant, the nitrogen ejecta quickly cools and forms knots. These knots are observed to have high velocities of ~ 9000 km s^{-1}. To achieve such high velocities, the nitrogen must have been near the surface of the star (where the shock velocity is high) when the star exploded.

Furthermore, the material is nitrogen rich but hydrogen poor. The N to Hα flux ratios are tens of times solar with just three exceptions. Most of the knots only have upper limits

for Hα flux. In order to have N/H $\sim 30\times$ solar, a typical limit for nitrogen-rich knots, the material must have undergone CNO processing until >90% of the hydrogen was depleted, but not have reached triple α burning temperatures (Arnett 1996, and references therein). When the star exploded, the He core must have been exposed, but not sufficiently eroded by mass loss to reach the C/O rich region.

Thus any progenitor must fit into a very narrow end-state, where most of the hydrogen envelope has been removed, but the C/O-rich core can not be exposed; the nitrogen is still in the star. The constraint on the progenitor is that it must have ended its life as a WN or WNL star. There is no other obvious way to produce these nitrogen knots, so we will take this constraint as solid.

3.2. Ejecta Mass

It would be useful to have a direct measurement of the mass of the star when it exploded. Though this is not possible, we can attempt an inventory of the material associated with Cas A today.

We begin with the mass of the ejecta expelled in the explosion. Estimating the ejecta mass is not straightforward. Previous research has used two principal methods. The first combines optical measurements of the positions of the forward and reverse shocks in the remnant with kinematic arguments to determine a mass and explosion energy (Chevalier & Oishi 2003; Laming & Hwang 2004). The one dimensional nature of these arguments in their present form and assumptions about the nature of the circumstellar medium and distribution of explosion energy introduce uncertainties into such estimates. Such calculations predict small ejecta masses in the 2-4 $M_\odot$ range.

The second estimate uses observations of the x-ray emitting gas (Willingale et al. 2002). X-ray spectral line fitting combined with emission models provides estimates of electron density and temperature, ion temperature, composition, and emissivity, which can be used to estimate the total amount of emitting material. The filling factor of the material, the ratio of ion to electron temperature $\frac{T_{ion}}{T_e}$, and the presence of a reservoir of material which is at a temperature where emission is inefficient can all change the mass estimate.

Both methods of determining the ejecta mass are very model dependent, but rely upon different sets of assumptions. The two methods both arrive at similar ejecta masses (2-4 $M_\odot$). Assuming that one method did not bias the other, and the errors in the two techniques have not led to the same incorrect answer, we can take this ejecta mass result as reasonably strong.

3.3. The Compact Remnant

To truly estimate the total mass of the star prior to collapse, we must also have an estimate of the compact remnant mass. If the compact remnant is a neutron star, we can set an upper limit to the remnant mass equal to the maximum neutron star mass. For most equations of state, this maximum neutron star mass for a slowly spinning neutron star is roughly $2.2\,M_{\odot}$ in baryons (i.e. Morrison, Baumgarte, & Shapiro 2004). If the compact remnant is a black hole, its mass is still weakly constrained by the nucleosynthetic yields (see §3.4). Depending upon the level of asymmetry in the explosion, the limit for a black hole could be as high as $5\,M_{\odot}$, opening up a much wider range in Cas A progenitors. Here we discuss the current evidence for the nature of the compact remnant.

The compact remnant of Cas A was discovered in the first-light image from the *Chandra* X-ray satellite (Tananbaum 1999). Since this time, observations from both the *Chandra* and XMM satellites have sought to pin down the nature of this remnant (Chakrabarty et al. 2001; Murray et al. 2002; Mereghetti, Tiengo, & Israel 2002). These observations, plus upper limits placed by observations in other wavelengths, have begun to constrain the nature of this compact remnant.

Chakrabarty et al. (2001) outlined the possible characteristics for the Cas A compact remnant: classical pulsar, accreting neutron star, accreting black hole, cooling neutron star, or anomalous X-ray pulsar/soft gamma-ray repeater (AXP/SGR). Due to the lack of a convincing detection of pulsations (Murray et al. 2002) and of any plerion, they conclude that it is unlikely the remnant is a classical, rapidly-spinning pulsar. This justifies our use of a maximum neutron star mass based on a slowly spinning neutron star. The optical to X-ray flux ratio strongly constrains accretion models. It is inconsistent with disk accretion in a normal low mass x-ray binary (LMXB), though accretion of SNR material may produce emission little like normal binary disk accretion. Models of accretion onto a weakly magnetized ($B < 10^9$ G) neutron star can produce the correct x-ray flux from the accretion boundary layer, but higher magnetic fields either prevent boundary layer formation or result in strong pulsations unless the NS is slowly rotating. The inner edge of a black hole accretion disk has too large an emitting area for x-rays, and advection dominated accretion flow (ADAF) and coronal models require fine-tuning (Chakrabarty et al. 2001). It should be noted that the correct value of the x-ray luminosity is dependent upon the interstellar absorption. At present the amount of absorption is model dependent (Chakrabarty et al. 2001, see Table 2 of). Pavlov et al. (2000) were forced to invoke extreme conditions to make a simple cooling model viable. Despite Cas A's X-ray luminosity being 3-10 times dimmer than the dimmest existing AXP, the AXP/SGR scenario fits the data reasonably well and it has become the favored remnant scenario for Cas A. This case has recently been strengthened by optical and

near IR limits from Fesen, Pavlov, & Sanwal (2005). Observations with NICMOS on HST detect no R, J, or H band counterpart to the compact object to magnitude limits of 28, 26.2, and 24.6, respectively.

Recently, Krause et al. (2005) have detected what they infer to be infrared echos arising from a 2×10^{46} erg outburst from the compact remnant. Assuming this burst of non-periodic emission arises from an SGR, this supports the idea that the remnant is an AXP/SGR. It would be difficult to explain such an outburst from an accretion scenario.

We can also place a lower limit on the neutron star mass. This limit is stronger to the extent that Cas A is a typical supernova rather than an odd event. It has long been known (i.e. Hainebach et al. 1974) that the dominant nuclei in the e-process are a sensitive function of the neutron excess η (or equivalently the electron fraction $Y_e = 0.5(1 - \eta)$). In order to reproduce the solar system isotopic abundances of Fe and Ni, a Y_e in the range of 1.5×10^{-3} to 3.0×10^{-3} is required (Arnett 1996, p270-272,321). This corresponds to $Y_e =$ 0.4992 to 0.4982. ^{56}Fe is produced as ^{56}Ni ($Z = N = 28$) which decays to ^{56}Fe through ^{56}Co. The most significant neutron-rich isotopes in the iron peak are ^{54}Fe ($Y_e = 0.485$) and ^{58}Ni ($Y_e = 0.483$). Requiring that they are produced in (at most) their solar system value gives $Y_e \geq 0.4982$. More neutron-rich material must not have been ejected in significant amounts. Figure 2 shows the electron fraction Y_e of the inner cores of our four progenitors. The matter interior to 1.75 $M_\odot$ [1] is too neutron-rich for the most massive progenitors, but this limit is relaxed to 1.5 $M_\odot$ or less for the lower mass progenitors. Although one could argue that the neutrinos streaming out of the proto-neutron star can reset Y_e, this is only true for matter very near the proto-neutron star surface. If Cas A is a peculiar object, such as the product of common envelope evolution and not a typical supernova, the Y_e argument is weakened to the extent that such objects rarely contribute to the ensemble of nucleosynthesis sources from which the solar system was derived. Very non-solar abundances relative to Fe might then be allowed, and the argument for the minimum mass for the neutron star remnant no longer holds.

[1]These are baryonic masses. Gravitational masses (measured in binary systems) are typically ∼10% less massive than baryonic masses. This mass deficit represent the gravitational binding energy of the object

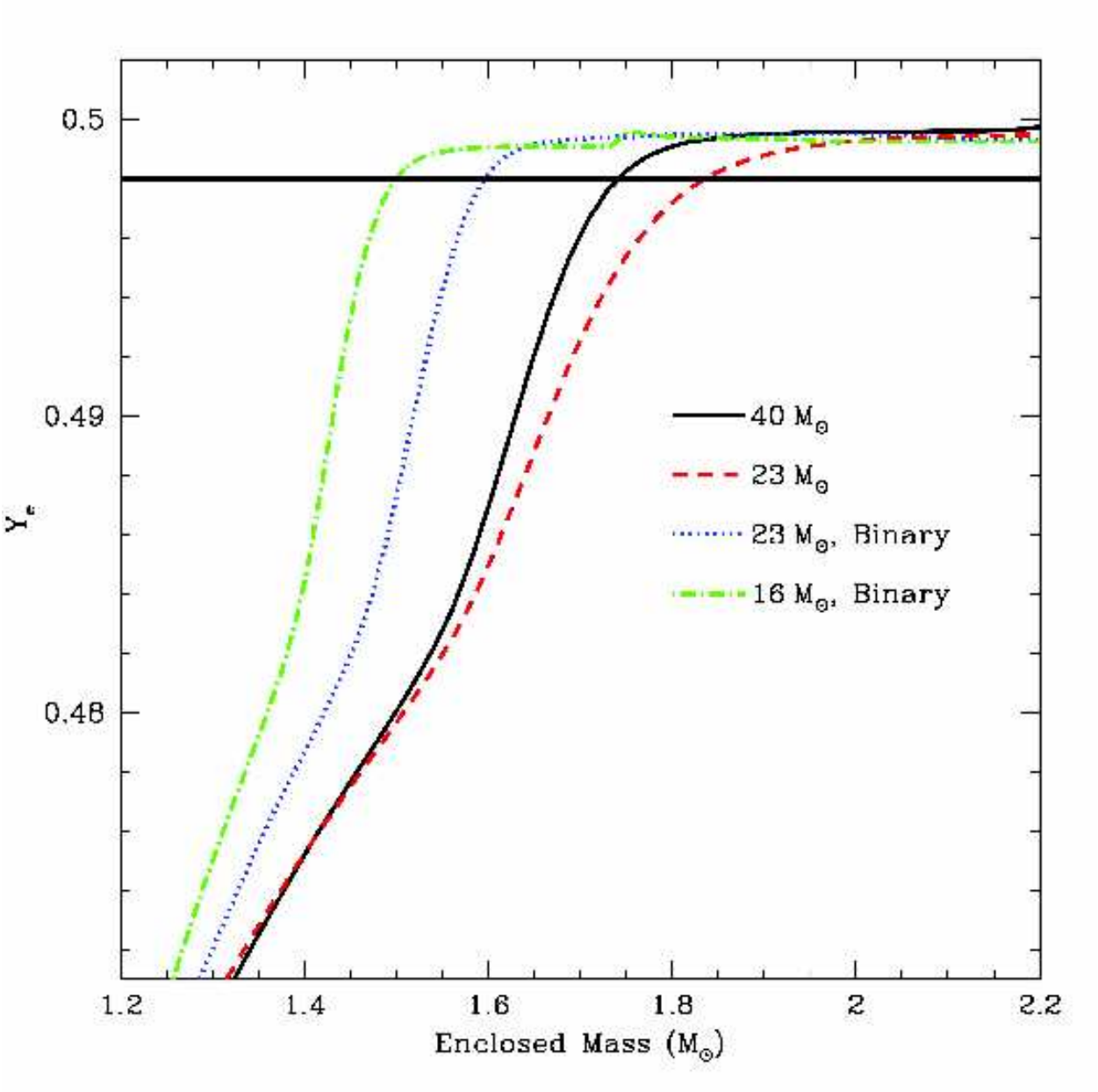

Fig. 2.— Y_e vs. enclosed mass for the four progenitor models. The lower the mass during Si burning, the smaller the neutron enriched core. The horizontal line indicates $Y_e = 0.498$, the approximate electron fraction for the solar iron peak. Very little material more neutron rich than this can be allowed to escape. This marks the minimum mass of the compact remnant compatible with galactic chemical evolution constraints.

Although we will consider a black hole remnant in this study, we note that the evidence is gradually increasing in support of a highly-magnetized, slowly-rotating, neutron star remnant for this object. We thus believe that the remnant mass is most likely below $2.2 M_{\odot}$.

3.4. ^{44}Ti and ^{56}Ni

As a final constraint, we consider the nucleosynthetic yields of both radioactive titanium ($^{44}\mathrm{Ti} \rightarrow {}^{44}\mathrm{Sc} \rightarrow {}^{44}\mathrm{Ca}$) and radioactive nickel ($^{56}\mathrm{Ni} \rightarrow {}^{56}\mathrm{Co} \rightarrow {}^{56}\mathrm{Fe}$). Nuclear decay lines from ^{44}Ca (1157 keV) and ^{44}Sc (67.9 and 78.4 keV) have been solidly detected towards Cas A with the CGRO COMPTEL and BeppoSAX PDS instruments, respectively (Iyudin et al. 1994; Iyudin 1997; Vink et al. 2001). These detections, when taken together, yield a line flux of $(2.5 \pm 1.0) \times 10^{-5}$photons cm^{-2} s^{-1}, which implies an initially synthesized mass of ^{44}Ti in the range of $(0.8 - 2.5) \times 10^{-4}$ $M_{\odot}$. Preliminary observations of the 68 keV line by ISGRI on INTEGRAL are consistent with the COMPTEL and BeppoSAX results (Vink 2005). This mass of ejected ^{44}Ti is generally thought to be abnormally large (or at best, marginally consistent) by comparison with spherical explosion models (Timmes et al. 1996).

To complicate the matter further, Timmes et al. (1996) argued that spherical explosion models with an ejected mass of $\sim 10^{-4}$ $M_{\odot}$ in ^{44}Ti would imply an ejected ^{56}Ni mass of at least 0.05 $M_{\odot}$. At the distance of Cas A, this should have resulted in a very bright supernova, yet historical records of the time show no such entry. Nagataki et al. (1998) point out that the $^{44}\mathrm{Ti}/^{56}\mathrm{Ni}$ ratio can vary substantially due to asymmetries in the explosion. We also find that the ration varies with the degree of asymmetry, and also with fallback and the initial composiution and thermodynamic trajectory of the material involved in α-rich freezeout. It has been suggested that the supernova associated with Cas A SNR was observed and recorded by J. Flamsteed in 1680 (Ashworth 1980) at a visual magnitude of 6. Unlike the ^{44}Ti, we have no solid constraints for the synthesized ^{56}Ni mass and must construct upper and lower limits from indirect evidence. In the remainder of this section, we consider constraints on the ^{56}Ni mass using two independent techniques. The first is based on an inventory of ^{56}Fe (the stable daughter product of ^{56}Ni) in the present day remnant, while the second relies on the absence of widespread reportage of the supernova event in astronomical records of the time.

A simple inventory of the X-ray emitting iron mass in Cas A has been presented by Willingale et al. (2003). They report an iron mass of 0.058 $M_{\odot}$ and argue convincingly that most of this iron originated in the supernova ejecta. With reasonable accuracy, we can assume this iron is comprised primarily of the ^{56}Fe isotope, which gives a relatively solid lower limit to the mass of radioactive ^{56}Ni that must have been synthesized and ejected by the

explosion. One could, in principle, attain an upper mass limit by assuming the mass interior to the reverse shock is made entirely of ^{56}Fe and then add the X-ray visible component to this number. However, as Hwang & Laming (2003) discuss, it is possible for there to be iron already hit by the reverse shock that we can no longer detect. As such, a solid constraint for the upper mass limit of ^{56}Ni poses a larger challenge and we turn instead to a constraint based on analytical lightcurve models.

Given the lack of widespread reportage of the event, we assume that the peak, visual magnitude was fainter than $m_v \sim 3$ (Da Silva 1993). For the general case, this includes the effect of visual extinction present at the time of the explosion. From this we can write down a simple expression for the absolute magnitude (M_{peak}) of the supernova at peak luminosity:

$$M_{peak} = 3 - A_v - 5\log\left(\frac{d}{10}\right) \tag{1}$$

where A_v is the magnitudes of visual extinction and d is the distance to Cas A (3.4 kpc).

Using the sun ($1\ L_\odot = 3.83 \times 10^{33}$erg s^{-1} and absolute magnitude of 4.83) as a standard, we can relate M_{peak} to a peak luminosity of the supernova in units of solar luminosity.

$$L_{peak} = 10^{(\frac{M_{peak}-4.83}{-2.5})} L_\odot \tag{2}$$

This leaves us with a maximum luminosity for the Cas A supernova in order to avoid widespread reportage. Our goal now is to derive through reasonable assumptions, the corresponding maximum mass of ^{56}Ni. Given the constraint on the ejecta mass, it is very likely that the $4-6\ M_\odot$ object that went supernova was initially of very small radius (as opposed to the standard red, supergiant progenitor.) With the assumption of small initial radius, we can employ a simple analytic model relating the supernova luminosity to its initial mass of ^{56}Ni (as described in Arnett (1982) and Pinto & Eastman (2000).) In essence, this model equates the peak luminosity with the instantaneous energy deposition from decay processes.

$$L_{peak} = M_{Ni}\Theta(t_{peak})\Lambda(t_{peak}) \tag{3}$$

where t_{peak} is the time at peak luminosity, M_{Ni} is the mass in grams of ^{56}Ni synthesized, Λ is essentially one minus the energy escape fraction of γ-rays and Θ is the instantaneous energy decay rate for the radioactive ^{56}Ni and ^{56}Co. Θ has units of erg s^{-1} g^{-1} and is given by

$$\Theta(t) = \frac{N_{av}}{56}\left(\frac{E_{Ni}}{\tau_{Ni}}e^{-t/\tau_{Ni}} + \frac{E_{Co}}{\tau_{Co}-\tau_{Ni}}\left(e^{-t/\tau_{Co}} - e^{-t/\tau_{Ni}}\right)\right) \quad (4)$$

where N_{av} is Avagadro's number, $\tau_{Ni} = 7.6 \times 10^5$ s, $\tau_{Co} = 9.6 \times 10^6$ s, $E_{Ni} = 1.73$ MeV and $E_{Co} = 3.69$ MeV are the mean decay lifetimes and energy per decay for ^{56}Ni and ^{56}Co respectively. A quantitative value for this upper mass limit of ^{56}Ni requires that we specify t_{peak} (the rise time to the peak of the light curve), $\Lambda(t_{peak})$ (the fraction of decay energy deposited at peak) and A_v (the magnitudes of visual extinction toward Cas A.)

We choose t_{peak} to be 18 days, which is a fairly typical rise time for Type Ib supernova lightcurves (Filippenko 1997). We adopt a value of 0.9 for $\Lambda(t_{peak})$ which is likely an underestimate. Since our intent here is to derive an upper limit for M_{Ni}, erring on the side of too little deposition is preferred. In order to check the validity of this assumption, we have run a γ-ray transport simulation (with the Maverick code; details in Hungerford, Fryer, & Warren (2003)) using our 16 and 40 $M_\odot$ progenitor models as input. The simulation results give a decay energy deposition of roughly 95% for the $16M_\odot$ and 100% for the $40M_\odot$ at t = 18.1 days. In order to reduce the deposition, the material must be more optically thin, which requires either a lower ejecta mass or very high expansion velocities. As such, the $16M_\odot$ model is our best case for the escapse of γ-rays, which supports our claim that 90% deposition is a cautious lower limit.

Current estimates for visual extinction values toward Cas A range from 4-8 magnitudes ((Peimbert & van den Bergh 1971; Troland, Crutcher & Heiles 1985; Predehl & Schmitt 1995) and reviews by Hartmann et al. (1997) and Diehl & Timmes (1998)). There has been discussion in the literature regarding the presence of a dust cloud at the time of the explosion, which has since been evaporated by passage of the supernova shock. Given the estimates for ejecta mass and swept-up mass in Willingale et al. (2003), any dust condensation which was present at the explosion and blasted away before the present epoch, was likely formed out of the wind material during the star's giant phase evolution. Typical extinction measurements toward WN stars possess visual extinctions which range all the way down to $A_v < 1$, suggesting that most of the extinction arises from the Galactic ISM rather than an intrinsic source (van der Hucht 2001). Also, CO measurements show that Cas A lies near two giant molecular clouds (GMCs) in the Perseus arm, and that extinction in the region will be large compared to a stellar dust contribution (Ungerechts, Umbanhowar, & Thaddeus 2000). This suggests that the extinction we see today is likely to be similar to that obscuring the explosion itself. If we adopt the larger end of this range (taken with $\Lambda = 0.9$ and $t_{peak} = 18$ days), we get a maximum mass for ^{56}Ni of 0.2 $M_\odot$.

Figure 3 plots ejected mass of ^{44}Ti against ^{56}Ni. The dotted line shows the solar ratio

of ^{44}Ca to ^{56}Fe, the principal decay products. The range allowed by the observations is shown by the stippled box. Our explosion calculations are shown by the dots. Model M23E2.3A (2.3 foe asymmetric explosion of 23 $M_\odot$ non-binary) rests in the upper right of the box. M23E2.0BinA (2.0 foe asymmetric explosion of 23 $M_\odot$ binary) falls in the lower left. The asymmetric and symmetric explosions of the 2.0 f.o.e. $23M_\odot$ binary and the 3.1 f.o.e. $16M_\odot$ binary have the same yields. This is because there is little fallback. The differences in abundance ratios in our other asymmetric models arise from differential fallback; some material gets out that would not escape in a symmetric explosion. Following the burning in 3D could change this result.

Clearly, the mass of ^{56}Ni is subject to uncertainty, and is, by far, the least stringent of our constraints. In addition, the predicted mass of both ^{56}Ni and ^{44}Ti are both very sensitive to the details of the explosion mechanism and calculation. Figure 3 shows that it is possible to produce reasonable abundances from an otherwise promising progenitor, but should not be taken to mean more than that. We do not believe these abundances can be used to distinguish between progenitor models at this stage.

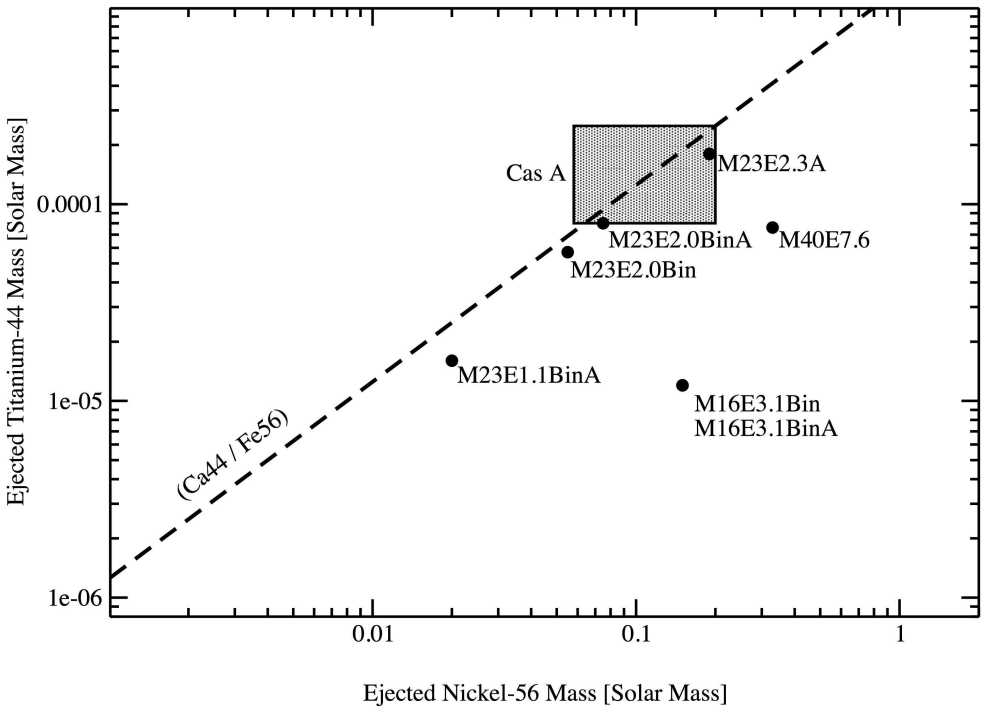

Fig. 3.— ejected mass of ^{44}Ti against ^{56}Ni. The range allowed by the observations is shown by the stippled box. Dots are our explosion calculations. Model M23E2.3A (2.3 foe asymmetric explosion of 23 $M_\odot$ non-binary) rests in the upper right of the box. M23E2.0BinA (2.0 foe asymmetric explosion of 23 $M_\odot$ binary) falls in the lower left. The dotted line shows the solar ratio of the principal decay products, ^{44}Ca and ^{56}Fe.

4. Observations versus Simulations

By reviewing the fate of our specific models, we can build up our intuition on what is (and is not) important in producing a viable Cas A progenitor. Table 2 shows the status of our models when compared against these observational constraints. We study each progenitor in turn.

Mass loss in the 40 $M_\odot$ progenitor removes all of the nitrogen rich material and a significant amount of C/O rich material. It cannot explain the nitrogen-rich knots. Also, because its final mass is over 6 $M_\odot$, it can not satisfy both the ejecta and remnant mass constraints. Increased mass loss during the LBV or WR phase could reduce the final mass to an acceptable value, but it would still fail to explain the N-rich knots. We ran a single very energetic explosion to fit the remnant mass. This explosion produced somewhat too much ^{56}Ni. A weaker explosion could fix this yield, but such a progenitor can never match the nitrogen-rich knots nor the total final mass constraints.

The single 23 $M_\odot$ progenitor suffers the same fate as the 40 $M_\odot$ star: it can not match either the nitrogen-rich knots or total final mass constraints. In this case the star retains a large hydrogen envelope. Increased mass loss which could strip the H envelope would have to occur as a luminous red supergiant. At this point the convective envelope has penetrated deeply into the star. The He burning convective core has also had more time to grow. Only a small ($\sim 0.1 M_\odot$) layer of pure CNO ashes remains between the convectively homogenized H-rich envelope and the C/O rich He burning shell. This layer has a mass coordinate of >8 $M_\odot$, depending on details of the mass loss history. We conclude that additional mass loss as an RSG would be unlikely to leave a He/N surface layer. We also notice another effect: to produce a neutron star, we almost invariably eject too much ^{56}Ni.

The binary 23 $M_\odot$ progenitor can marginally match all the data. It requires a strong enough explosion to make a neutron star, but if the explosion is strong enough, it appears that both the ^{44}Ti and ^{56}Ni yields both lie within our set of constraints. Note that although the 2×10^{51} erg explosion with a mild asymmetry can explain everything, the compact remnant is on the massive end. A better fit would probably arise from a slightly more energetic explosion.

The binary 16 $M_\odot$ progenitor can also marginally match all of the data except for the ^{44}Ti. It fits nicely within the total mass constraints, but has difficulty reproducing the yields. A strong explosion produces enough ^{56}Ni but too little ^{44}Ti, while a weak one produces too little of both ^{44}Ti and ^{56}Ni. It would appear that a binary model somewhere between 16 and 23 $M_\odot$ with a moderately energetic explosion could fit the constraints well. It is worth noting, however, that there are significant uncertainties in the predicted yields.

5. Possible Progenitors

In this section we present a series of options for the progenitor's identity as we descend the decision tree of constraints. The strongest of the constraints is the presence of fast-moving Nitrogen-rich, hydrogen-poor ejecta. At the time of the explosion, the star's surface composition was mostly CNO processed ash. There does not appear to be any way to avoid this conclusion, and all of our options will follow from it. We do not separately consider the nucleosynthesis constraints. They are weaker observationally than the other constraints, and the nucleosynthesis is far too model dependent to be a good discriminator between otherwise viable alternatives.

A high mass Wolf-Rayet progenitor (such as our 40 $M_\odot$ progenitor) will uncover its C/O core before core-collapse. The observation of nitrogen-rich knots excludes such a progenitor. Unfortunately, uncertainties in LBV and Wolf-Rayet mass-loss rates make it difficult for us to place an upper limit on the progenitor mass due to this constraint. Our conservative estimate for this limit is 28-30 $M_\odot$.

For single stars, we can also place a lower limit on the progenitor mass. Low mass stars will not lose their hydrogen envelope by core collapse. For example, by the time the 23 $M_\odot$ single-star model reaches the red giant branch it has lost less than 3 $M_\odot$, leaving almost 10 $M_\odot$ still in the hydrogen rich envelope. The star does lose a further 6 solar masses, and it is conceivable that our mass loss rates may be off by a factor of two for red supergiants. However, we know that some stars in the 15 -25 $M_\odot$ mass range retain a hydrogen envelope from the example of SN87A. Even if the mass loss is sufficient to strip the envelope, most of it must occur when the star is a luminous red supergiant, meaning that the convective envelope has penetrated deeply into the star, and the He burning convective core is large. Only a small ($\sim 0.1 M_\odot$) layer of pure CNO ashes remains between the H-rich envelope and the C/O rich He burning shell. It would require considerable fine tuning to time core collapse to coincide with the short period during which such a star would have CNO ash-rich surface layers. In addition, this layer has a mass coordinate of >8 $M_\odot$ for a 23 $M_\odot$ progenitor, well outside the predicted size of the Cas A progenitor. For binary systems, this lower limit on the mass is removed, since the H envelope can be removed early.

The first branching point for progenitor options rests upon the estimates of total ejecta mass. From Section 3.2 above, the ejecta mass has been estimated from similarity solutions constrained by the positions of the optical forward and reverse shocks and from x-ray spectral fits. Both of these methods produce similar values for the ejecta mass (2-4 $M_\odot$), but both are also model dependent. As we show below, relaxing this constraint fundamentally changes the parameter space available for a progenitor. Detailed modeling and additional observations which would provide a more secure and complete determination of the ejecta

mass are desirable.

5.1. High Ejecta Mass

If we take the view that the mass determinations quoted above represent a lower limit on some incompletely sampled mass of ejecta, we are given more options for a progenitor. In this case it is possible to admit a high mass star ($> 30\ M_{\odot}$)which has evolved into a WN or WNL star through single star evolution. Such a star could produce a neutron star remnant with a sufficiently energetic explosion, but would produce at least six solar masses of O-rich ejecta. Alternatively it could produce less ejecta and a black hole remnant with a weaker explosion. We may think of this as a "normal" Type Ib SN.

5.2. Low Ejecta Mass

If we accept that the current inventories of ejecta mass are substantially complete and accurate, we are left with two options for a progenitor which depend upon the nature of the compact object. The sum of mass in the ejecta and compact remnant give us the total mass of the star at core collapse. We present two options, one for a neutron star compact remnant and one for a black hole.

5.2.1. Black Hole Remnant

This scenario is the least constraining of our final two options. A somewhat arbitrary amount of mass can be incorporated into a black hole, so we have only weak constraints on the mass of the star at collapse. Much as in the high ejecta mass model, we are allowed a more massive progenitor which can produce a WN or WNL star from single star evolution. In this case a weak explosion with a large amount of fallback produces$\sim 2\ M_{\odot}$ of ejecta and a $\lesssim 6\ M_{\odot}$ black hole, again allowing progenitors $< 30\ M_{\odot}$. Such weak explosions would have difficulty producing enough ^{44}Ti and ^{56}Ni.

5.2.2. Neutron Star Remnant

If we accept all of our observational constraints to this point at face value we arrive at this scenario. Current work on neutron star equations of state place an upper limit on

neutron star masses of $\sim 2.2\ M_\odot$. The neutron star plus the observational estimates of ejecta mass give us a total mass at core collapse of $\sim$ 4-6 $M_\odot$.

The very low mass at collapse, combined with the N-rich, H-poor surface composition, imply a unique progenitor for Cas A. Massive Wolf-Rayet progenitors have triple α processed cores which are too large. Mass loss would uncover C/O rich material well before reducing the core to 6 $M_\odot$. A lower mass star which retains a hydrogen envelope until the RSG stage will mix the CNO processed material with H-rich envelope material during dredge-up. Only a thin layer of CNO ash at the hydrogen burning shell remains, leaving a problem of fine-tuned timing if a star with such a small core can remove its entire hydrogen envelope at all.

We require a scenario in which a relatively low mass star ($< 25\ M_\odot$), which would not ordinarily produce a WN star, loses all or most of its envelope early in its post main sequence evolution. Wolf Rayet mass loss is then sufficient to reduce the star to its final small mass while retaining a CNO processed outer layer. The immediately obvious way to achieve this is to invoke common envelope evolution in a binary.

Our 23 $M_\odot$ progenitor with "binary envelope ejection" can produce a massive neutron star and 4 $M_\odot$ of ejecta with a reasonable explosion energy. The total core mass at explosion of 6.4 $M_\odot$ puts it at the massive end of the range allowed by the observational ejecta mass determinations and theoretical neutron star equations of state. An explosion energy above $\sim 2 \times 10^{51}$ erg would be able to explain all our constraints at the upper mass extreme of our constraints. A lower mass star ($\sim 16\ M_\odot$) which undergoes a common envelope phase resides more comfortably with the parameter space, with a final core mass of 5 $M_\odot$, though it has difficulty producing the correct amount of ^{44}Ti and ^{56}Ni. Details of the envelope ejection and subsequent mass loss can shift these mass estimates slightly.

We are left with a low mass ($15< M <25\ M_\odot$) binary progenitor. Chance would appear to have made our most easily studied young supernova remnant a peculiar member of its class, rather than a truly representative Rosetta stone. This very peculiarity however, probably gives us much more insight into the progenitor and the nature of the explosion.

6. Implications

The findings of this study have broader implications for both Cas A in particular and supernovae in general. If we accept all of the available observational constraints, the progenitor of Cas A turns out to be atypical. A low mass star masquerading as a Wolf Rayet after losing its envelope to a binary interaction is not an ideal model for "normal" supernovae, but

may be more common than we think, given the high binary frequency of massive stars. On the other hand, its oddness may help to pin down the nature of the progenitor much better than would otherwise be possible. This could remove some of the uncertainties normally unavoidable in modeling the explosion, making simulations a much more powerful tool for understanding the explosion mechanism. We have laid out arguments for further refining the constraints by both theoretical and observational means.

If the progenitor to Cas A was indeed a binary, then we are faced with new issues. We would expect the binary interaction to give rise to significant asymmetries in the circumstellar medium which should be imprinted on the structure of the remnant. While Cas A shows marked asymmetry in the northeast and southwest jet-like features, these appear to be associated with the explosion and not the interaction with the surrounding medium. The density of fast moving knots appears to be lower in the north and south edges of the remnant (Fesen 2001), and there is some evidence of interaction with dense material at the edge (Fesen 2001; Hines et al. 2004, i.e.), but there is no glaring evidence of bipolar structure.

Asymmetries associated with binary interaction can show up in two places. The first is the post-envelope ejection fast wind, which is associated with the quasi-stationary flocculi (QSFs) (Fesen & Becker 1991). There are three reasons why we might not see evidence of asymmetry in this wind: 1) Cas A was not a binary at all; 2) an accident of geometry placed our line of sight along an axis of symmetry; 3) the companion star merged with the progenitor during the common envelope phase.

The second place where a binary would generate asymmetry is where the expanding remnant runs into the ejected envelope. If the shock has impacted this material we should see the emission, so reason two above does not help us. Two simple scenarios are capable of addressing this problem. Let us consider the mass swept up by the ISM.

$$\begin{aligned} \dot{M} &\simeq 4\pi r^2 v \rho_{ISM} \\ \rho_{ISM} &\simeq n_H/A \\ \tfrac{M}{M_\odot} &\simeq \tfrac{4\pi}{3}(vt)^2 vt \tfrac{n_H}{M_\odot A} \\ \tfrac{M}{M_\odot} &\simeq 13 n_H (\tfrac{v}{50\mathrm{km\ s^{-1}}})^3 (\tfrac{t}{10^5\mathrm{yr}})^3 \end{aligned} \tag{5}$$

where $\frac{M}{M_\odot}$ is the mass swept up, n_H is the number density of hydrogen, and A is Avogadro's number.

Assuming an ejection velocity for the envelope of 50 km s^{-1} at 10^5 yr before the explosion, the ejected material will have reached 5 pc by the time the star exploded, if the surrounding area already has $n_H \ll 1$, i.e. in a bubble swept out by an OB association. The age and velocity both represent conservative estimates for a star on the first ascent RGB, so

it is quite possible that the SNR simply has not yet encountered the envelope in this scenario. At the opposite extreme, the envelope could have impacted a very dense ISM, for example a molecular cloud, at an early time. The kinetic energy of the envelope would be very small compared to the inertia of the ISM, and would have imposed very little asymmetry. Any forward shock would have dissipated quickly, and the reverse shock would have long since propagated back to the origin, so we would see no obvious evidence of that interaction at the present time. In this scenario the SNR may already have propagated through the WR wind bubble and be interacting with a combined envelope/ISM. Estimates of the mass swept up by the remnant and indications of an interaction with a molecular cloud tend to support the latter idea, but this is an area which would benefit from additional observational scrutiny along with multi-D simulation of the interaction between winds, SNRs, and the ISM.

Detailed calculations of nucleosynthesis during the explosion will be discussed in a subsequent paper, but this work already demonstrates that estimates of yields are subject to severe uncertainties. We note a few of these here as a prelude to the detailed calculations. Not surprisingly, mixing of material during the explosion can drastically change the yield of species produced deep in the star. A 1D explosion with a mass cut cannot predict yields correctly. For example, a 3D code will give larger Ti and Ni yields than 1D. This can mean the difference between several hundredths of a solar mass of Ni and none at all.

Nuclear processing and adjustments to statistical equilibrium can continue for tens of seconds. We find that several effects can result in $1-2$ orders of magnitude changes in the abundance of species such as ^{44}Ti. For example, it is common to follow nuclear burning for $\sim$ 5s after the explosion. In these calculations the time to completion of the freeze-out process was of order tens of seconds. Not surpirsingly, the α network used in the explosion calculation produces a much larger yield of $Z = N$ species (most notably ^{44}Ti and ^{56}Ni) than the larger post-processing network. We also discovered that the choice of time at which we cut out the neutron star and replaced it with a hard inner boundary had an effect of similar magnitude on the yields. The choice of explosion energy, which is arbitrary so long as it doesn't contradict observational determinations of the energetics, produces large changes, as does any imposed asymmetry. We are forced to the conclusion that a much larger and more thorough effort must be made to understand the theoretical uncertainties in the yields before the observed yields can be used as a meaningful constraint.

The primary location of Ni production is also debatable. It is common in the observational literature to state that ^{56}Ni is produced by $\alpha-$rich freezeout of material from the progenitor's Si shell. This is not at all clear. One zone nucleosynthesis models starting with compositions taken from our progenitor models show a wide variety of final compositions which depend sensitively upon both the initial entropy and the thermodynamic trajectory

of the material. Often these compositions are not dominated by ^{56}Ni; a very small neutron excess is sufficient to poison the freezeout. Because of the importance of even a small neutron excess, substantial post processing is necessary. Results from an alpha network cannot be taken at face value. It is common to "reset" Y_e in the progenitor to remove the neutron excess. Neutrinos may be able to reset Y_e, but much of the material in which neutrino deposition could occur falls back onto the compact object in our simulations. It may be that most of the Z=N material is produced by alpha rich freezeout from the oxygen shell. The fate of the Si shell must be calculated in detail for a given specific case. A great deal of systematic theoretical work must be done before yields from an explosion can be considered reliable.

The results of the explosions are very sensitive to the choice of progenitor models. Mixing, mass loss, neutrino processes, non-spherical displacements and perturbations, and angular momentum can all influence the explosion, and all are imperfectly to poorly understood. Aspects of the progenitor evolution are discussed in Young et al. (2005), and effects that appear only in multi-D in Meakin, Young, & Arnett (submitted). These uncertainties in the initial conditions exacerbate the unknowns of the explosion mechanism itself.

In spite of this, by taking advantage of the constraints we have on the progenitor of Cas A, we can now use additional observations to better understand the supernova explosion mechanism. The explosion energy of the Cas A supernova is predicted to be at the high end of the range expected for normal supernovae: $2 - 4 \times 10^{51}$ erg (e.g. Chevalier & Oishi (2003)).

Fryer & Kalogera (2001) examine how supernova explosion energy varies with mass. They argued that the supernova explosion energy peaked for $15M_\odot$ progenitors. At $23M_\odot$, they predicted an explosion energy of less than 10^{51} erg. The progenitors we have used in this paper are very different than the progenitors used in the work by Fryer & Kalogera (2001). Those progenitors assumed single stars with *no* mass loss, and the code used more approximate prescriptions for nuclear burning and convection. Instead of comparing star mass, it is better to compare the fate of stars with specific structures. Figure 4 compares the accretion rate onto the outer part of the convective region during collapse (Fryer et al. (1999) describes why this particular structure information is ideal in comparing progenitors) for our 16 and $23M_\odot$ stars against the 15 and $25M_\odot$ from Fryer & Kalogera (2001). Already, knowing that a strong explosion can be produced for stars with structures lying between our 16 and $23M_\odot$ binary progenitors provides some of the most accurate limits on the supernova explosion mechanism currently available. As we restrict our range of possible progenitors and place stronger constraints on the explosion energy and yields, we provide a very stringent test for any core-collapse code. In this sense, Cas A now can play an active role in validating

core-collapse codes.

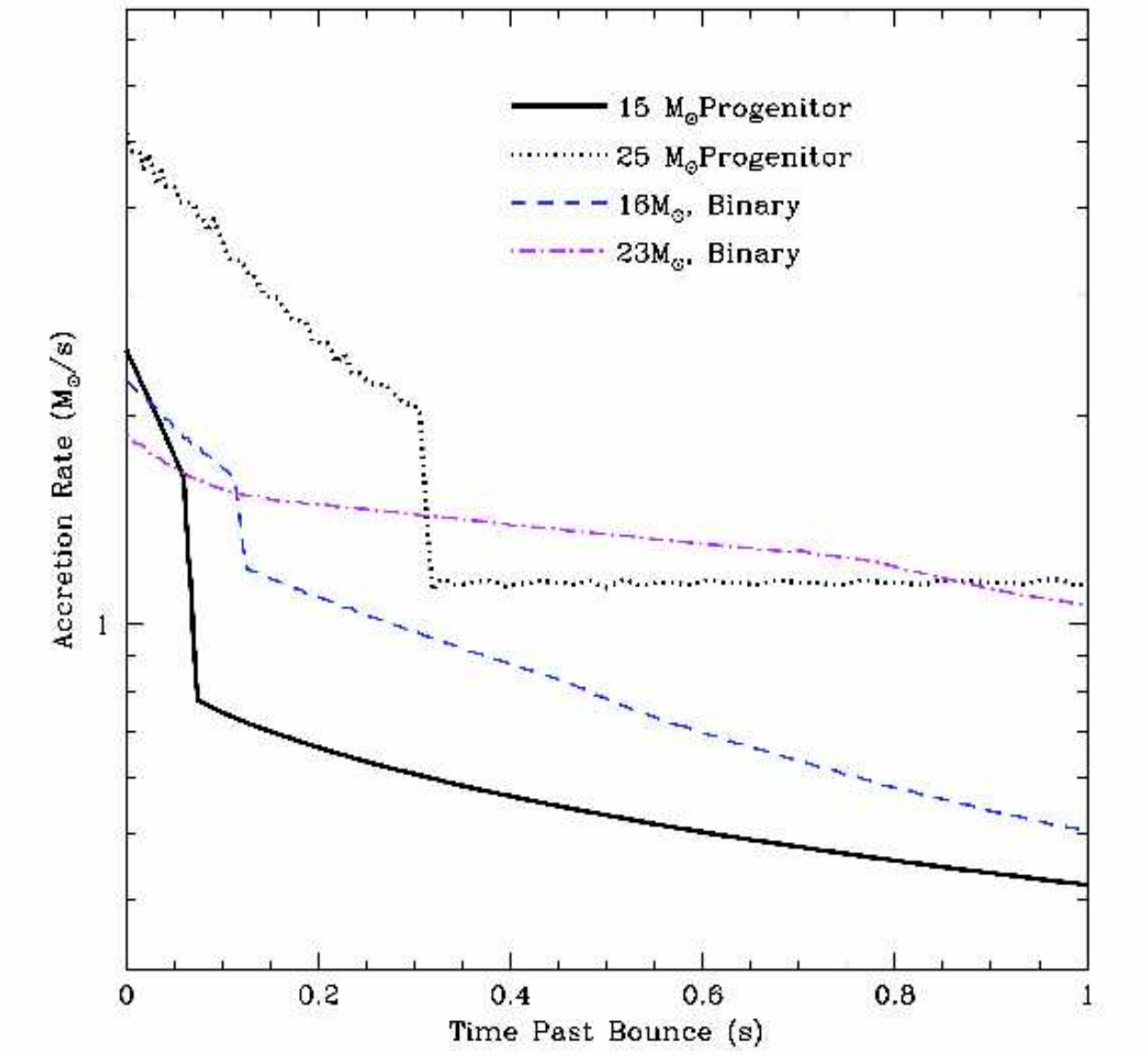

Fig. 4.— Accretion rate vs. time since bounce for the 16 and 23 $M_\odot$ binary models from this paper and 15 and 25 $M_\odot$ single stars from Fryer & Kalogera (2001). The time of the sharp drop determines the timing and the accretion rate the energy of the explosion. Energetic explosions are allowable in the region bounded by the 15 and 25 $M_\odot$ models. A binary model between 16 and 23 $M_\odot$ can satisfy the prediction of an energetic explosion (Chevalier & Oishi 2003).

This work was funded in part under the auspices of the U.S. Dept. of Energy, and supported by its contract W-7405-ENG-36 to Los Alamos National Laboratory, by a DOE SciDAC grant DE-FC02-01ER41176, an NNSA ASC grant, and a subcontract to the ASCI FLASH Center at the University of Chicago. BV thanks the Eugene McDermott Scholarship Program for support during the summer of 2005 at Los Alamos National Laboratory when this work was completed.

REFERENCES

Arnett, W. David 1982, ApJ, 253, 785

Arnett, David 1996, *Supernovae and Nucleosynthesis*, Princeton University Press

Ashworth, W. B. 1980, J. Hist. Astron., 11, 1

Benz, W., Thielemann, F.-K., & Hills, J. G. 1989, ApJ, 342, 986

Blair, William P. et al. 2000, ApJ, 537, 667

Blöcker, T. 1995, A&A, 297, 727

Chakrabarty, Deepto, Pivovaroff, Michael J., Hernquist, Lars E., Heyl, Jeremy S., & Narayan, Ramesh 2001, ApJ, 548, 800

Chevalier, Roger A. & Oishi, Jeffrey 2003, ApJ, 593, 23

Da Silva, L. A. L. 1993, Ap&SS, 202, 215

Diehl, Roland & Timmes, F. X. 1998, Publications of the Astronomical Society of the Pacific, 110, 637

Fesen, Robert A. & Becker, Robert H. 1991, ApJ, 371, 621

Fesen, Robert A. 2001, ApJS, 133, 161

Fesen, R. A., Pavlov, G. G., & Sanwal, D. 2005, astro-ph/0509552

Filippenko, A. V. 1997, ARA&A, 35, 309

Fryer, C. L., Burrows, A., & Benz, W. 1998, ApJ, 496, 333

Fryer, Chris L. 1999, ApJ, 522, 413

Fryer, Chris, Benz, Willy, Herant, Marc, & Colgate, Stirling A. 1999, ApJ, 516, 892

Fryer, Chris, L. & Kalogera, Vasiliki 2001, ApJ, 554, 548

Fryer, C. L., Rockefeller, G., & Warren, M. S. 2005, ApJ, submitted

Grevesse, N. & Sauval, A. J., 1998, Space Science Reviews, 85, 161

Hainebach, K. L., Clayton, D. D., Arnett, W. D., & Woosley, S. E. 1974, ApJ, 193, 157

Hartmann, D. H., Predehl, P., Greiner, J., Egger, J., Trümper, J., Aschenbach, B., Iyudin, A. F., Diehl, R. D., Oberlack, U., Schönfelder, V., Leising, M. D., The, L.-S., Timmes, F. X., Woosley, S. E., Hoffman, R., Langer, N., & Garcia-Segura, G. 1997, Nuclear Physics A, 621, 83c

Herant, Marc, Benz, Willy, Hix, W. Raphael, Fryer, Chris L., & Colgate, Stirling A. 1994, ApJ, 435, 339

Hines, D. C. et al. 2004, ApJS, 154, 290

Hungerford, Aimee L., Fryer, Chris L., & Warren, Michael S. 2003, ApJ, 594, 390

Hwang, Una & Laming, J. Martin 2003, ApJ, 597, 362

Iyudin, A., Diehl, R., Bloemen, H., Hermsen, W., Lichti, G., Morris, D., Ryan, J., Shoenfelder, V., Steinle, H., Varendorff, M., de Vries, C., & Winkler, C. 1994, A&A, 284L, 1

Iyudin, A. 1997, Nuclear Physics A, 654, 900c

Krause, Oliver et al. 2005, Science, 308, 1604

Kudritzki, R. P., Pauldrach, A., Puls, J., & Abbott, D. C. 1989, A&A, 219, 205

Lamers, H. J. G. L. M. & Nugis, T. 2003, A&A, 395L, 1

Laming, J. Martin & Hwang, Una 2003, ApJ, 597, 347

Meakin, Casey, Young, Patrick A., & Arnett, David 2005, ApJ, submitted

Mereghetti, S., Tiengo, A., & Israel, G. L. 2002, ApJ, 569, 275

Morrison, Ian A., Baumgarte, Thomas W., & Shapiro, Stuart L. 2004, ApJ, 610, 941

Murray, Stephen S., Ransom, Scott M., Juda, Michael, Hwang, Una, & Holt, Stephen S. 2002, ApJ, 566, 1039

Nagataki, Shigehiro, Hashimoto, Masa-Aki, Sato, Katsuhiko, Yamada, Shoichi, & Mochizuki, Yuko S. 1998, ApJ, 492L, 45

Pavlov, G. G., Zavlin, V. E., Aschenbach, B., Trümper, J., & Sanwal, D. 2000, ApJ, 531, 53

Peimbert, M. & van den Bergh, S. 1971, ApJ, 167, 223

Pinto, P. A. & Eastman, R. G. 2000, ApJ, 530, 744

Predehl, P. & Scmitt, J. H. M. M. 1995, A&A, 293, 889

Reed, J. E., Hester, J. J., Fabian, A. C., & Winkler, P. F. 1995, ApJ, 440, 706

Tananbaum, H. 1999, IAU Circ.7246

Thorstensen, John R., Fesen, Robert A., & van den Bergh, Sidney 2001, AJ, 122, 297

Timmes, F. X., Woosley, S. E., Hartmann, D. H., & Hoffman, R. D. 1996 ApJ, 464, 332

Troland, T. H., Crutcher, R. M., & Heiles, C. 1985, ApJ, 298, 808

Ungerechts, H., Umbanhowar, P., & Thaddeus, P. 2000, ApJ, 537, 221

van der Hucht, Karl, A. 2001, NewAR, 45, 135

Vink, J., Laming, J. M., Kaastra, J., Bleeker, J., Bloemen, H., & Oberlack, U. 2001, ApJ, 560, 79

Vink, Jacco 2005, AdSpR, 35, 976

Willingale, R., Bleeker, J. A. M., van der Heyden, K. J., Kaastra, J. S., & Vink, J. 2002, A&A, 381, 1039

Willingale, R., Bleeker, J. A. M., van der Heyden, K. J., & Kaastra, J. S. 2003, A&A, 398, 1021

Young, Patrick A. & Arnett, David 2005, ApJ, 618, 908

Young, Patrick A., Meakin, Casey, Arnett, David, & Fryer, Chris L. 2005, ApJ, 629, 101

Table 1. Explosion Simulations

Simulation	M_{Prog} ($M_\odot$)	Energy 10^{51} erg	Bin.	Asym. Jet2[a]	M_{Rem} ($M_\odot$)	M_{Ejecta} ($M_\odot$)	^{44}Ti Yield ($M_\odot$)	^{56}Ni Yield ($M_\odot$)
M40E7.6	40	7.6	N	N	1.75	6.0	7.5×10^{-5}	0.33
M23E0.8	23	0.8	N	N	5.4	7.5	$< 10^{-5}$	$< 10^{-5}$
M23E2.3	23	2.3	N	N	4.6	8.3	1.2×10^{-5}	2.6×10^{-4}
M23E2.3A	23	2.3	N	Y	5.5	7.4	1.8×10^{-4}	0.19
M23E1.1Bin	23	1.1	Y	N	2.6	3.6	1.2×10^{-5}	2.6×10^{-4}
M23E1.1BinA	23	1.1	Y	Y	3.2	3.0	1.6×10^{-5}	0.02
M23E2.0Bin	23	2.0	Y	N	2.3	3.9	5.7×10^{-5}	0.055
M23E2.0BinA	23	2.0	Y	Y	2.6	3.6	8.0×10^{-5}	0.075
M16E1.3Bin	16	1.3	Y	N	1.8	3.25	$< 10^{-5}$	$< 10^{-5}$
M16E1.1BinA	16	1.12	Y	Y	1.85	3.2	$< 10^{-5}$	$< 10^{-5}$
M16E3.1Bin	16	3.1	Y	N	1.18	3.87	1.2×10^{-5}	0.15
M16E3.1BinA	16	3.1	Y	Y	1.19	3.86	1.2×10^{-5}	0.15

[a]See Hungerford, Fryer, & Warren (2003) for details.

Table 2. Simulation vs. Constraints

Simulation	Nitrogen Clumps	Ejecta Mass	Remnant Mass	^{44}Ti Yield	^{56}Ni Yield
M40E7.6	N	N	Y	Y	Y?
M23E0.8	N	N	N	N	N
M23E2.3	N	N	N	N	N
M23E2.3A	N	N	N	Y	Y
M23E1.1Bin	Y	Y	Y?	N	N
M23E1.1BinA	Y	Y	N	N	Y
M23E2.0Bin	Y	Y	Y?	Y?	Y
M23E2.0BinA	Y	Y	Y?	Y	Y
M16E1.3Bin	Y	Y	Y	N	N
M16E1.1BinA	Y	Y	Y	N	N
M16E3.1Bin	Y	Y	Y	N	Y
M16E3.1BinA	Y	Y	Y	N	Y